

# Space-time Galerkin isogeometric method and efficient solver for parabolic problem\*

G. Loli<sup>†</sup>

M. Montardini<sup>†</sup>

G. Sangalli<sup>†‡</sup>

M. Tani<sup>‡</sup>

July 29, 2022

## Abstract

In this work we focus on the preconditioning of a Galerkin space-time isogeometric discretization of the heat equation. Exploiting the tensor product structure of the basis functions, we propose a preconditioner that is the sum of Kronecker products of matrices and that can be efficiently applied thanks to an extension of the classical fast diagonalization method. The preconditioner is robust w.r.t. polynomial degree and the time required for the application is almost proportional to the number of degrees-of-freedom, for a serial execution. By incorporating some information on the geometry parametrization and on the coefficients, we keep high efficiency with non-trivial geometry parametrization of the domain.

**Keywords:** Isogeometric analysis, splines, heat equation, space-time Galerkin formulation, fast diagonalization.

## 1 Introduction

Isogeometric analysis (IGA), introduced in the seminal paper [15] (see also the book [4]), is an evolution of classical finite element methods. IGA uses spline functions, or their generalizations, both to represent the computational domain and to approximate the solution of the partial differential equation that models the problem of interest. This is meant to simplify the interoperability between computer aided design and numerical simulations. Isogeometric analysis also benefits from the approximation properties of splines, whose high-continuity yields higher accuracy when compared to  $C^0$  piecewise polynomials, see e.g., [8, 3, 25].

In this paper we focus on the heat equation and on its space-time Galerkin isogeometric discretization. Space-time finite element methods originated in the papers [10, 16, 23] and, typically, adopt a discontinuous approximation in time, since this produces a time marching algorithm with a traditional step-by-step format (see e.g. [26]). Our work, instead, explores the use of smooth approximation in space and time. We focus in particular on the plain Galerkin space-time method, whose well-posedness has been studied, for finite element discretizations and for the heat equation, in the recent papers [28] and [29]. A key issue, when adopting smooth approximation in space and time, is the design of an efficient solver for the space-time system, which is inherently global. This is indeed the aim of this paper. Exploiting the tensor product structure of the spline basis and assuming that the spatial domain does not change with time, the linear system has the structure

$$\gamma \mathbf{W}_t \otimes \mathbf{M}_s + \nu \mathbf{M}_t \otimes \mathbf{K}_s, \quad (1.1)$$

where  $\mathbf{W}_t$  is given by the Galerkin discretization of the time derivative,  $\mathbf{K}_s$  is given by the discretization of the Laplacian in the spatial variables,  $\mathbf{M}_t$  and  $\mathbf{M}_s$  are “mass matrices” in time and space, respectively, and  $\gamma, \nu > 0$  are constants of the problem. Adopting an iterative solver, we do not need to form the matrix (1.1) (observe that the cost of formation of the matrices in (1.1) is comparable to the cost of forming a steady-state diffusion matrix) but there is the need of an efficient preconditioning strategy. The main contribution of this paper is the construction of a the preconditioner for (1.1) generalizing the classical fast diagonalization method [20]. Indeed the fast diagonalization, as other fast solvers for (1.1), would require the eigendecomposition of the pencil  $(\mathbf{W}_t, \mathbf{M}_t)$  which is numerically unstable. We circumvent this difficulty by introducing an ad-hoc factorization of

\*Version of July 29, 2022

<sup>†</sup>Università di Pavia, Dipartimento di Matematica “F. Casorati”, Via A. Ferrata 1, 27100 Pavia, Italy.

<sup>‡</sup>IMATI-CNR “Enrico Magenes”, Pavia, Italy.

Emails: {gabriele.loli01, monica.montardini01}@universitadipavia.it, giancarlo.sangalli@unipv.it, mattia.tani@imati.cnr.it

the time matrices which allows to design a solver conceptually similar to the fast diagonalization method. The computational cost of the setup of the resulting preconditioner is  $O(N_{dof})$  floating-point operations (FLOPs) while its application is  $O(N_{dof}^{1+1/d})$  FLOPs, where  $d$  is the number of spatial dimensions and  $N_{dof}$  denotes the total number of degrees-of-freedom (assuming, for simplicity, to have the same number of degrees-of-freedom in time and in each spatial direction). Our numerical benchmarks show that the computing time (serial and single-core execution) is close to optimality, that is, proportional to  $N_{dof}$ . The preconditioner is robust with respect to the polynomial degree. Furthermore, our approach is optimal in terms of memory requirement: denoting by  $N_s$  the total number of degrees-of-freedom in space, the storage cost is  $O(p^d N_s + N_{dof})$ . We also remark that global space-time methods in principle facilitate the full parallelization of the solver, see [7, 12, 18].

The work [21] is similar to this one but the Galerkin formulation is replaced by a  $L^2$  least-squares variational formulation: this has the advantage that the classical fast diagonalization can be used directly to construct a suitable preconditioner (as in the elliptic case, see [24]). A comparison of the two approaches is carried out in this paper, showing the higher efficiency of the plain Galerkin method.

Other papers in literature propose isogeometric space-time Galerkin methods but favour a step-by-step structure in time. In [19], the space-time domain is decomposed into space-time slabs that are sequentially coupled in time by a stabilized discontinuous Galerkin method. Related multigrid solvers have been proposed in [13, 14]. In [2] the authors consider  $C^0$  coupling between the space-time slabs with a suitable stabilized formulation that also yields to a sequential scheme. Space-time isogeometric analysis involving fluid-structure interaction, again based on discontinuous approximation in time, are proposed in [30, 31, 32].

The outline of the paper is as follows. In Section 2 we present the basics of B-splines and isogeometric analysis. The model problem and its IGA discretization are introduced in Section 3, while in Section 4 we define the preconditioner and we discuss its application. We present the numerical results assessing the performance of the proposed preconditioner in Section 5. Finally, in the last section we draw some conclusions and we highlight some future research directions.

## 2 Preliminaries

### 2.1 B-Splines

Given  $m$  and  $p$  two positive integers, a knot vector in  $[0, 1]$  is a sequence of non-decreasing points  $\Xi := \{0 = \xi_1 \leq \dots \leq \xi_{m+p+1} = 1\}$ . We consider open knot vectors, i.e. we set  $\xi_1 = \dots = \xi_{p+1} = 0$  and  $\xi_m = \dots = \xi_{m+p+1} = 1$ . Then, according to Cox-De Boor recursion formulas (see [5]), univariate B-splines  $\hat{b}_{i,p} : (0, 1) \rightarrow \mathbb{R}$  are piecewise polynomials defined as

for  $p = 0$ :

$$\hat{b}_{i,0}(\eta) = \begin{cases} 1 & \text{if } \xi_i \leq \eta < \xi_{i+1}, \\ 0 & \text{otherwise,} \end{cases}$$

for  $p \geq 1$ :

$$\hat{b}_{i,p}(\eta) = \begin{cases} \frac{\eta - \xi_i}{\xi_{i+p} - \xi_i} \hat{b}_{i,p-1}(\eta) + \frac{\xi_{i+p+1} - \eta}{\xi_{i+p+1} - \xi_{i+1}} \hat{b}_{i+1,p-1}(\eta) & \text{if } \xi_i \leq \eta < \xi_{i+p+1}, \\ 0 & \text{otherwise,} \end{cases}$$

where we adopt the convention  $0/0 = 0$ . The univariate spline space is defined as

$$\hat{\mathcal{S}}_h^p := \text{span}\{\hat{b}_{i,p}\}_{i=1}^m,$$

where  $h$  denotes the mesh-size, i.e.  $h := \max_{i=1,\dots,m+p} \{|\xi_{i+1} - \xi_i|\}$ . The interior knot multiplicity influences the smoothness of the B-splines at the knots (see [5]). For more details on B-splines properties and their use in IGA we refer to [4].

Multivariate B-splines are defined as tensor product of univariate B-splines. We consider functions that depend on  $d$  spatial variables and the time variable. Therefore we introduce  $d+1$  univariate knot vectors  $\Xi_l := \{\xi_{l,1} \leq \dots \leq \xi_{l,m_l+p_l+1}\}$  for  $l = 1, \dots, d$  and  $\Xi_t := \{\xi_{t,1} \leq \dots \leq \xi_{t,m_t+p_t+1}\}$ . Let  $h_s$  be the maximal meshsize in all spatial knot vectors and let  $h_t$  be the meshsize of the time knot vector. Let  $\mathbf{p}$  be the vector that

contains the degree indexes, i.e.  $\mathbf{p} := (\mathbf{p}_s, p_t)$ , where  $\mathbf{p}_s := (p_s, \dots, p_s) \in \mathbb{N}^d$ , that is, we assume to have the same polynomial degree in all spatial directions.

We assume that the following quasi-uniformity of the knot vectors holds.

**Assumption 1.** *There exists  $0 < \alpha \leq 1$ , independent of  $h_s$  and  $h_t$ , such that each non-empty knot span  $(\xi_{l,i}, \xi_{l,i+1})$  fulfills  $\alpha h_s \leq \xi_{l,i+1} - \xi_{l,i} \leq h_s$  for  $1 \leq l \leq d$  and each non-empty knot-span  $(\xi_{t,i}, \xi_{t,i+1})$  fulfills  $\alpha h_t \leq \xi_{t,i+1} - \xi_{t,i} \leq h_t$ .*

The multivariate B-splines are defined as

$$\widehat{B}_{\mathbf{i}, \mathbf{p}}(\boldsymbol{\eta}, \tau) := \widehat{B}_{\mathbf{i}_s, \mathbf{p}_s}(\boldsymbol{\eta}) \widehat{b}_{i_t, p_t}(\tau),$$

where

$$\widehat{B}_{\mathbf{i}_s, \mathbf{p}_s}(\boldsymbol{\eta}) := \widehat{b}_{i_1, p_s}(\eta_1) \dots \widehat{b}_{i_d, p_s}(\eta_d), \quad (2.1)$$

$\mathbf{i}_s := (i_1, \dots, i_d)$ ,  $\mathbf{i} := (\mathbf{i}_s, i_t)$  and  $\boldsymbol{\eta} = (\eta_1, \dots, \eta_d)$ . The corresponding spline space is defined as

$$\widehat{\mathcal{S}}_h^{\mathbf{p}} := \text{span} \left\{ \widehat{B}_{\mathbf{i}, \mathbf{p}} \mid i_k = 1, \dots, m_k \text{ for } k = 1, \dots, d; i_t = 1, \dots, m_t \right\},$$

where  $h := \max\{h_s, h_t\}$ . We have that  $\widehat{\mathcal{S}}_h^{\mathbf{p}} = \widehat{\mathcal{S}}_{h_s}^{\mathbf{p}_s} \otimes \widehat{\mathcal{S}}_{h_t}^{p_t}$ , where  $\widehat{\mathcal{S}}_{h_s}^{\mathbf{p}_s} := \text{span} \left\{ \widehat{B}_{\mathbf{i}_s, \mathbf{p}_s}(\boldsymbol{\eta}) \mid i_k = 1, \dots, m_k \text{ for } k = 1, \dots, d \right\}$  is the space of tensor-product splines on  $\widehat{\Omega} := (0, 1)^d$ .

**Assumption 2.** *We assume that  $p_t, p_s \geq 1$  and that  $\widehat{\mathcal{S}}_{h_s}^{\mathbf{p}_s} \subset C^0(\widehat{\Omega})$  and  $\widehat{\mathcal{S}}_{h_t}^{p_t} \subset C^0((0, 1))$ .*

## 2.2 Isogeometric spaces

The space-time computational domain that we consider is  $\Omega \times (0, T)$ , where  $\Omega \subset \mathbb{R}^d$  and  $T > 0$  is the final time. We make the following assumption.

**Assumption 3.** *We assume that  $\Omega$  is parametrized by  $\mathbf{F} : \widehat{\Omega} \rightarrow \Omega$ , with  $\mathbf{F} \in \left[ \widehat{\mathcal{S}}_{h_s}^{\mathbf{p}_s} \right]^d$ . Moreover, we assume that  $\mathbf{F}^{-1}$  has piecewise bounded derivatives of any order.*

We define  $\mathbf{x} = (x_1, \dots, x_d) := \mathbf{F}(\boldsymbol{\eta})$  and  $t := T\tau$ . Then space-time domain is given by the parametrization  $\mathbf{G} : \widehat{\Omega} \times (0, 1) \rightarrow \Omega \times (0, T)$ , such that  $\mathbf{G}(\boldsymbol{\eta}, \tau) := (\mathbf{F}(\boldsymbol{\eta}), T\tau) = (\mathbf{x}, t)$ .

We introduce the spline space with initial and boundary conditions, in parametric coordinates, as

$$\widehat{\mathcal{X}}_h := \left\{ \widehat{v}_h \in \widehat{\mathcal{S}}_h^{\mathbf{p}} \mid \widehat{v}_h = 0 \text{ on } \partial\widehat{\Omega} \times (0, 1) \text{ and } \widehat{v}_h = 0 \text{ on } \widehat{\Omega} \times \{0\} \right\}.$$

We also have that  $\widehat{\mathcal{X}}_h = \widehat{\mathcal{X}}_{h_s} \otimes \widehat{\mathcal{X}}_{h_t}$ , where

$$\begin{aligned} \widehat{\mathcal{X}}_{h_s} &:= \left\{ \widehat{w}_h \in \widehat{\mathcal{S}}_{h_s}^{\mathbf{p}_s} \mid \widehat{w}_h = 0 \text{ on } \partial\widehat{\Omega} \right\} = \text{span} \left\{ \widehat{b}_{i_1, p_s} \dots \widehat{b}_{i_d, p_s} \mid i_k = 2, \dots, m_k - 1; k = 1, \dots, d \right\}, \\ \widehat{\mathcal{X}}_{h_t} &:= \left\{ \widehat{w}_h \in \widehat{\mathcal{S}}_{h_t}^{p_t} \mid \widehat{w}_h(0) = 0 \right\} = \text{span} \left\{ \widehat{b}_{i_t, p_t} \mid i_t = 2, \dots, m_t \right\}. \end{aligned}$$

By introducing a colexicographical reordering of the basis functions, we can write

$$\begin{aligned} \widehat{\mathcal{X}}_{h_s} &= \text{span} \left\{ \widehat{b}_{i_1, p_s} \dots \widehat{b}_{i_d, p_s} \mid i_k = 1, \dots, n_{s,k}; k = 1, \dots, d \right\} = \text{span} \left\{ \widehat{B}_{\mathbf{i}, \mathbf{p}_s} \mid i = 1, \dots, N_s \right\}, \\ \widehat{\mathcal{X}}_{h_t} &= \text{span} \left\{ \widehat{b}_{i_t, p_t} \mid i_t = 1, \dots, n_t \right\} \end{aligned}$$

and then

$$\widehat{\mathcal{X}}_h = \text{span} \left\{ \widehat{B}_{\mathbf{i}, \mathbf{p}} \mid i = 1, \dots, N_{dof} \right\}, \quad (2.3)$$

where  $n_t := m_t - 1$ ,  $n_{s,k} := m_k - 2$ ,  $N_s := \prod_{k=1}^d n_{s,k}$ ,  $N_{dof} := N_s n_t$ .

Finally, the isogeometric space we consider is the isoparametric push-forward of (2.3) through the geometric map  $\mathbf{G}$ , i.e.

$$\mathcal{X}_h := \text{span} \left\{ B_{\mathbf{i}, \mathbf{p}} := \widehat{B}_{\mathbf{i}, \mathbf{p}} \circ \mathbf{G}^{-1} \mid i = 1, \dots, N_{dof} \right\}. \quad (2.4)$$

We also have that  $\mathcal{X}_h = \mathcal{X}_{h_s} \otimes \mathcal{X}_{h_t}$ , where

$$\mathcal{X}_{h_s} := \text{span} \left\{ B_{\mathbf{i}, \mathbf{p}_s} := \widehat{B}_{\mathbf{i}, \mathbf{p}_s} \circ \mathbf{F}^{-1} \mid i = 1, \dots, N_s \right\}, \quad \mathcal{X}_{h_t} := \text{span} \left\{ b_{i_t, p_t} := \widehat{b}_{i_t, p_t}(\cdot/T) \mid i_t = 1, \dots, n_t \right\}.$$

### 2.3 Kronecker product

The Kronecker product of two matrices  $\mathbf{C} \in \mathbb{C}^{n_1 \times n_2}$  and  $\mathbf{D} \in \mathbb{C}^{n_3 \times n_4}$  is defined as

$$\mathbf{C} \otimes \mathbf{D} := \begin{bmatrix} [\mathbf{C}]_{1,1}\mathbf{D} & \dots & [\mathbf{C}]_{1,n_2}\mathbf{D} \\ \vdots & \ddots & \vdots \\ [\mathbf{C}]_{n_1,1}\mathbf{D} & \dots & [\mathbf{C}]_{n_1,n_2}\mathbf{D} \end{bmatrix} \in \mathbb{C}^{n_1 n_3 \times n_2 n_4},$$

where the  $ij$ -th entry of the matrix  $\mathbf{C}$  is denoted by  $[\mathbf{C}]_{i,j}$ . For extensions and properties of the Kronecker product we refer to [17]. In particular, when a matrix has a Kronecker product structure, the matrix-vector product can be efficiently computed. For this purpose, define, for  $m = 1, \dots, d+1$ , the  $m$ -mode product  $\times_m$  of a tensor  $\mathfrak{X} \in \mathbb{C}^{n_1 \times \dots \times n_{d+1}}$  with a matrix  $\mathbf{J} \in \mathbb{C}^{\ell \times n_m}$  as a tensor of size  $n_1 \times \dots \times n_{m-1} \times \ell \times n_{m+1} \times \dots \times n_{d+1}$  whose elements are

$$[\mathfrak{X} \times_m \mathbf{J}]_{i_1, \dots, i_{d+1}} = \sum_{j=1}^{n_m} [\mathfrak{X}]_{i_1, \dots, i_{m-1}, j, i_{m+1}, \dots, i_{d+1}} [\mathbf{J}]_{i_m, j}.$$

Then, given  $\mathbf{J}_i \in \mathbb{C}^{\ell_i \times n_i}$  for  $i = 1, \dots, d+1$ , it holds

$$(\mathbf{J}_{d+1} \otimes \dots \otimes \mathbf{J}_1) \text{vec}(\mathfrak{X}) = \text{vec}(\mathfrak{X} \times_1 \mathbf{J}_1 \times_2 \dots \times_{d+1} \mathbf{J}_{d+1}), \quad (2.5)$$

where the vectorization operator “ $\text{vec}$ ” applied to a tensor stacks its entries into a column vector as

$$[\text{vec}(\mathfrak{X})]_j = [\mathfrak{X}]_{i_1, \dots, i_{d+1}} \text{ for } i_l = 1, \dots, n_l \text{ and for } l = 1, \dots, d+1,$$

where  $j := i_1 + \sum_{k=2}^{d+1} [(i_k - 1)\Pi_{l=1}^{k-1} n_l]$ .

## 3 The model problem

### 3.1 Space-time variational formulation

Our model problem is the heat equation: we look for a solution  $u$  such that

$$\begin{cases} \gamma \partial_t u - \nabla \cdot (\nu \nabla u) &= f & \text{in } \Omega \times (0, T), \\ u &= 0 & \text{on } \partial\Omega \times [0, T], \\ u &= u_0 & \text{in } \Omega \times \{0\}, \end{cases} \quad (3.1)$$

where  $\Omega \subset \mathbb{R}^d$ ,  $T$  is the final time,  $\gamma > 0$  is the heat capacity constant and  $\nu > 0$  is the thermal conductivity constant. We assume that  $f \in L^2(0, T; H^{-1}(\Omega))$  and that  $u_0 \in L^2(\Omega)$ . This last assumption guarantees the existence of a lifting  $\bar{u}_0$  of  $u_0$  such that  $\bar{u}_0 \in L^2(0, T; H_0^1(\Omega)) \cap H^1(0, T; H^{-1}(\Omega))$ , see [9]. We introduce the Hilbert spaces

$$\mathcal{X} := \{v \in L^2(0, T; H_0^1(\Omega)) \cap H^1(0, T; H^{-1}(\Omega)) \mid v(\mathbf{x}, 0) = 0\} \quad \text{and} \quad \mathcal{Y} := L^2(0, T; H_0^1(\Omega)),$$

endowed with the following norms

$$\|v\|_{\mathcal{X}}^2 := \frac{\gamma^2}{\nu} \|\partial_t v\|_{L^2(0, T; H^{-1}(\Omega))}^2 + \nu \|v\|_{L^2(0, T; H_0^1(\Omega))}^2 \quad \text{and} \quad \|v\|_{\mathcal{Y}}^2 := \nu \|v\|_{L^2(0, T; H_0^1(\Omega))}^2,$$

respectively. The variational formulation of (3.1) reads:

$$\text{Find } u \in \mathcal{X} \text{ such that } \mathcal{A}(u, v) = \mathcal{F}_0(v) := \mathcal{F}(v) - \mathcal{A}(\bar{u}_0, v) \quad \forall v \in \mathcal{Y}, \quad (3.2)$$

where the bilinear form  $\mathcal{A}(\cdot, \cdot)$  and the linear form  $\mathcal{F}(\cdot)$  are defined as

$$\mathcal{A}(v, w) := \int_0^T \int_{\Omega} (\gamma \partial_t v w + \nu \nabla v \cdot \nabla w) \, d\Omega \, dt \quad \text{and} \quad \mathcal{F}(w) := \int_0^T \int_{\Omega} f w \, d\Omega \, dt \quad \forall v \in \mathcal{X} \text{ and } \forall w \in \mathcal{Y}.$$

The well-posedness of the variational formulation above is a classical result, see for example [28].

### 3.2 Space-time Galerkin method

Let  $\mathcal{X}_h \subset \mathcal{X}$  be the isogeometric space defined in (2.4). We consider the following Galerkin method for (3.2):

$$\text{Find } u_h \in \mathcal{X}_h \text{ such that } \mathcal{A}(u_h, v_h) = \mathcal{F}_0(v_h) \quad \forall v_h \in \mathcal{X}_h. \quad (3.3)$$

Following [28], let  $N_h : L^2(0, T; H^{-1}(\Omega)) \rightarrow \mathcal{X}_h$  be the discrete Newton potential operator: given  $\phi \in L^2(0, T; H^{-1}(\Omega))$  then  $N_h \phi \in \mathcal{X}_h$  fulfills

$$\int_0^T \int_{\Omega} \nu \nabla(N_h \phi) \nabla v_h \, d\Omega \, dt = \gamma \int_0^T \int_{\Omega} \phi v_h \, d\Omega \, dt \quad \forall v_h \in \mathcal{X}_h.$$

Thus, we define the norm in  $\mathcal{X}_h$  as

$$\|w\|_{\mathcal{X}_h}^2 := \nu \|N_h(\partial_t w)\|_{L^2(0, T; H_0^1(\Omega))}^2 + \nu \|w\|_{L^2(0, T; H_0^1(\Omega))}^2.$$

The stability and the well-posedness of the formulation (3.3) are guaranteed by a straightforward extension to IGA of [28, Equation (2.7)], [28, Theorem 3.1] and [28, Theorem 3.2].

**Proposition 1.** *It holds*

$$\mathcal{A}(w, v) \leq \sqrt{2} \|w\|_{\mathcal{X}} \|v\|_{\mathcal{Y}} \quad \forall w \in \mathcal{X} \text{ and } \forall v \in \mathcal{Y},$$

and

$$\|w_h\|_{\mathcal{X}_h} \leq 2\sqrt{2} \sup_{v_h \in \mathcal{X}_h} \frac{\mathcal{A}(w_h, v_h)}{\|v_h\|_{\mathcal{Y}}} \quad \forall w_h \in \mathcal{X}_h.$$

**Theorem 1.** *There exists a unique solution  $u_h \in \mathcal{X}_h$  to the discrete problem (3.3). Moreover, it holds*

$$\|u - u_h\|_{\mathcal{X}_h} \leq 5 \inf_{w_h \in \mathcal{X}_h} \|u - w_h\|_{\mathcal{X}},$$

where  $u \in \mathcal{X}$  is the solution of (3.2).

We have then the following a-priori estimate for  $h$ -refinement.

**Theorem 2.** *Let  $q$  be an integer such that  $1 \leq q \leq \min\{p_s, p_t\} + 1$ . If  $u \in \mathcal{X} \cap H^1(0, T; H^q(\Omega)) \cap H^q(0, T; H^1(\Omega))$  is the solution of (3.2) and  $u_h \in \mathcal{X}_h$  is the solution of (3.3), then it holds*

$$\|u - u_h\|_{\mathcal{X}_h} \leq C \sqrt{\frac{\gamma^2}{\nu} + \nu} \left( h_s^{q-1} \|u\|_{H^1(0, T; H^q(\Omega))} + h_t^{q-1} \|u\|_{H^q(0, T; H^1(\Omega))} \right) \quad (3.4)$$

where  $C$  is independent of  $h_s, h_t, \gamma, \nu$  and  $u$ .

*Proof.* We use the approximation estimates of the isogeometric spaces from [1]. We report here only the main steps, since the proof is similar to the one of [21, Proposition 4].

Let  $u \in \mathcal{X} \cap H^1(0, T; H^q(\Omega)) \cap H^q(0, T; H^1(\Omega))$ . Let  $\Pi_h u$  be a suitable projection of  $u$  in  $\mathcal{X}_h$ , based on the construction of [1]. We have the a-priori bounds

$$\begin{aligned} \|\partial_t(u - \Pi_h u)\|_{L^2(0, T; H^{-1}(\Omega))} &\leq C_1 \|\partial_t(u - \Pi_h u)\|_{L^2(0, T; L^2(\Omega))} \\ &\leq C_2 \left( h_s^{q-1} \|u\|_{H^1(0, T; H^{q-1}(\Omega))} + h_t^{q-1} \|u\|_{H^q(0, T; L^2(\Omega))} \right), \end{aligned}$$

and also

$$\|u - \Pi_h u\|_{L^2(0, T; H_0^1(\Omega))} \leq C_3 \left( h_s^{q-1} \|u\|_{L^2(0, T; H^q(\Omega))} + h_t^{q-1} \|u\|_{H^{q-1}(0, T; H^1(\Omega))} \right).$$

Therefore, we get

$$\|u - \Pi_h u\|_{\mathcal{X}}^2 \leq C_4 \left( \frac{\gamma^2}{\nu} + \nu \right) \left[ h_s^{2(q-1)} \|u\|_{H^1(0, T; H^q(\Omega))}^2 + h_t^{2(q-1)} \|u\|_{H^q(0, T; H^1(\Omega))}^2 \right]$$

which gives (3.4) thanks to Theorem 1. The constants  $C_1, C_2, C_3$  and  $C_4$  above are independent of  $h_s, h_t, \gamma, \nu$  and  $u$ .  $\square$

**Remark 1.** *The constants in the estimates of Proposition 1 and of Theorem 1 can be improved by considering a different norm in the functional space  $\mathcal{X}$ , i.e. by choosing  $\|v\|^2 := \|v\|_{\mathcal{X}}^2 + \gamma \|v(T)\|_{L^2(\Omega)}^2$ , as remarked in [28, 29].*

### 3.3 Discrete system

The linear system associated to (3.3) is

$$\mathbf{A} \mathbf{u}_h = \mathbf{F}, \quad (3.5)$$

where  $[\mathbf{A}]_{i,j} = \mathcal{A}(B_{j,\mathbf{p}}, B_{i,\mathbf{p}})$  and  $[\mathbf{F}]_i = \mathcal{F}_0(B_{i,\mathbf{p}})$ . The tensor-product structure of the isogeometric space (2.4) allows to write the system matrix  $\mathbf{A}$  as sum of Kronecker products of matrices as

$$\mathbf{A} = \gamma \mathbf{W}_t \otimes \mathbf{M}_s + \nu \mathbf{M}_t \otimes \mathbf{K}_s, \quad (3.6)$$

where for  $i, j = 1, \dots, n_t$

$$[\mathbf{W}_t]_{i,j} = \int_0^T b'_{j,p_t}(t) b_{i,p_t}(t) dt \quad \text{and} \quad [\mathbf{M}_t]_{i,j} = \int_0^T b_{i,p_t}(t) b_{j,p_t}(t) dt, \quad (3.7a)$$

while for  $i, j = 1, \dots, N_s$

$$[\mathbf{K}_s]_{i,j} = \int_{\Omega} \nabla B_{i,\mathbf{p}_s}(\mathbf{x}) \cdot \nabla B_{j,\mathbf{p}_s}(\mathbf{x}) d\Omega \quad \text{and} \quad [\mathbf{M}_s]_{i,j} = \int_{\Omega} B_{i,\mathbf{p}_s}(\mathbf{x}) B_{j,\mathbf{p}_s}(\mathbf{x}) d\Omega. \quad (3.7b)$$

## 4 Preconditioner definition and application

We introduce, for the system (3.5), the preconditioner

$$[\widehat{\mathbf{A}}]_{i,j} := \widehat{\mathcal{A}}(\widehat{B}_{j,\mathbf{p}}, \widehat{B}_{i,\mathbf{p}}),$$

where

$$\widehat{\mathcal{A}}(\widehat{v}, \widehat{w}) := \int_0^1 \int_{\widehat{\Omega}} (\gamma \partial_t \widehat{v} \widehat{w} + \nu \nabla \widehat{v} \cdot \nabla \widehat{w}) d\widehat{\Omega} d\tau \quad \forall \widehat{v}, \widehat{w} \in \widehat{\mathcal{X}}_h.$$

We have again

$$\widehat{\mathbf{A}} = \gamma \widehat{\mathbf{W}}_t \otimes \widehat{\mathbf{M}}_s + \nu \widehat{\mathbf{M}}_t \otimes \widehat{\mathbf{K}}_s, \quad (4.1)$$

where  $\widehat{\mathbf{W}}_t$ ,  $\widehat{\mathbf{K}}_t$ ,  $\widehat{\mathbf{K}}_s$  and  $\widehat{\mathbf{M}}_s$  are the equivalent of (3.7a) and (3.7b), respectively, in the parametric domain, i.e. for  $i, j = 1, \dots, n_t$

$$[\widehat{\mathbf{W}}_t]_{i,j} = \int_0^1 \widehat{b}'_{j,p_t}(\tau) \widehat{b}_{i,p_t}(\tau) d\tau \quad \text{and} \quad [\widehat{\mathbf{M}}_t]_{i,j} = \int_0^1 \widehat{b}_{i,p_t}(\tau) \widehat{b}_{j,p_t}(\tau) d\tau, \quad (4.2a)$$

while for  $i, j = 1, \dots, N_s$

$$[\widehat{\mathbf{K}}_s]_{i,j} = \int_{\widehat{\Omega}} \nabla \widehat{B}_{i,\mathbf{p}_s}(\boldsymbol{\eta}) \cdot \nabla \widehat{B}_{j,\mathbf{p}_s}(\boldsymbol{\eta}) d\widehat{\Omega} \quad \text{and} \quad [\widehat{\mathbf{M}}_s]_{i,j} = \int_{\widehat{\Omega}} \widehat{B}_{i,\mathbf{p}_s}(\boldsymbol{\eta}) \widehat{B}_{j,\mathbf{p}_s}(\boldsymbol{\eta}) d\widehat{\Omega}. \quad (4.2b)$$

Thanks to (2.1), the spatial matrices (4.2b) have the following structure

$$\widehat{\mathbf{K}}_s = \sum_{k=1}^d \widehat{\mathbf{M}}_d \otimes \dots \otimes \widehat{\mathbf{M}}_{k+1} \otimes \widehat{\mathbf{K}}_k \otimes \widehat{\mathbf{M}}_{k-1} \otimes \dots \otimes \widehat{\mathbf{M}}_1 \quad \text{and} \quad \widehat{\mathbf{M}}_s = \widehat{\mathbf{M}}_d \otimes \dots \otimes \widehat{\mathbf{M}}_1, \quad (4.3)$$

where for  $k = 1, \dots, d$  and for  $i, j = 1, \dots, n_{s,k}$

$$[\widehat{\mathbf{K}}_k]_{i,j} := \int_0^1 \widehat{b}'_{i,p_s}(\eta_k) \widehat{b}'_{j,p_s}(\eta_k) d\eta_k \quad \text{and} \quad [\widehat{\mathbf{M}}_k]_{i,j} := \int_0^1 \widehat{b}_{i,p_s}(\eta_k) \widehat{b}_{j,p_s}(\eta_k) d\eta_k.$$

The efficient application of the proposed preconditioner, that is, the solution of a system with matrix  $\widehat{\mathbf{A}}$ , should exploit the structure highlighted above. When the pencils  $(\widehat{\mathbf{W}}_t, \widehat{\mathbf{M}}_t)$ ,  $(\widehat{\mathbf{K}}_1, \widehat{\mathbf{M}}_1), \dots, (\widehat{\mathbf{K}}_d, \widehat{\mathbf{M}}_d)$  admit a stable generalized eigendecomposition, a possible approach is the fast diagonalization (FD) method, see [6] and [20] for details. We will see in Section 4.1 that the spatial pencils  $(\widehat{\mathbf{K}}_1, \widehat{\mathbf{M}}_1), \dots, (\widehat{\mathbf{K}}_d, \widehat{\mathbf{M}}_d)$  admit a stable diagonalization, but this is not the case of  $(\widehat{\mathbf{W}}_t, \widehat{\mathbf{M}}_t)$ , that needs a special treatment as explained in Section 4.2.

## 4.1 Stable factorization of the pencils $(\widehat{\mathbf{K}}_i, \widehat{\mathbf{M}}_i)$ $i = 1, \dots, d$

The spatial stiffness and mass matrices  $\widehat{\mathbf{K}}_i$  and  $\widehat{\mathbf{M}}_i$  are symmetric and positive definite. Thus, the pencils  $(\widehat{\mathbf{K}}_i, \widehat{\mathbf{M}}_i)$  for  $i = 1, \dots, d$  admit the generalized eigendecomposition

$$\widehat{\mathbf{K}}_i \mathbf{U}_i = \widehat{\mathbf{M}}_i \mathbf{U}_i \boldsymbol{\Lambda}_i \quad (4.4)$$

where the matrices  $\mathbf{U}_i$  contain in each column the  $\widehat{\mathbf{M}}_i$ -orthonormal generalized eigenvectors, and  $\boldsymbol{\Lambda}_i$  are diagonal matrices whose entries contain the generalized eigenvalues. Therefore we have for  $i = 1, \dots, d$  the factorizations

$$\mathbf{U}_i^T \widehat{\mathbf{K}}_i \mathbf{U}_i = \boldsymbol{\Lambda}_i \quad \text{and} \quad \mathbf{U}_i^T \widehat{\mathbf{M}}_i \mathbf{U}_i = \mathbb{I}_{n_{s,i}}, \quad (4.5)$$

where  $\mathbb{I}_{n_{s,i}}$  denotes the identity matrix of dimension  $n_{s,i} \times n_{s,i}$ . The stability of the decomposition (4.5) is expressed by the condition number of the eigenvector matrix. In particular  $\mathbf{U}_i^T \widehat{\mathbf{M}}_i \mathbf{U}_i = \mathbb{I}_{n_{s,i}}$  implies that

$$\kappa_{\widehat{\mathbf{M}}_i}(\mathbf{U}_i) := \|\mathbf{U}_i\|_{\widehat{\mathbf{M}}_i} \|\mathbf{U}_i^{-1}\|_{\widehat{\mathbf{M}}_i} = 1,$$

where  $\|\cdot\|_{\widehat{\mathbf{M}}_i}$  is the norm induced by the vector norm  $\|\mathbf{v}\|_{\widehat{\mathbf{M}}_i} := (\mathbf{v}^T \widehat{\mathbf{M}}_i \mathbf{v})^{1/2}$  for  $\mathbf{v} \in \mathbb{R}^{n_{s,i}}$ . Furthermore,

$$\kappa_2(\mathbf{U}_i) := \|\mathbf{U}_i\|_2 \|\mathbf{U}_i^{-1}\|_2 = \sqrt{\kappa_2(\widehat{\mathbf{M}}_i)},$$

where  $\|\cdot\|_2$  is the norm induced by the euclidean vector norm. The condition number  $\kappa_2(\widehat{\mathbf{M}}_i)$  has been studied in [11] and it does not depend on  $n_{sub}$  but it depends on the polynomial degree. Indeed, we report in Table 1 the behavior of  $\kappa_2(\mathbf{U}_i)$  that exhibits a dependence only on the degree  $p_s$ , but stays moderately low for all low polynomial degrees that are in the range of interest.

$n_{sub}$	$p_s = 2$	$p_s = 3$	$p_s = 4$	$p_s = 5$	$p_s = 6$	$p_s = 7$	$p_s = 8$
32	$2.7 \cdot 10^0$	$4.5 \cdot 10^0$	$7.6 \cdot 10^0$	$1.3 \cdot 10^1$	$2.1 \cdot 10^1$	$3.5 \cdot 10^1$	$5.7 \cdot 10^1$
64	$2.7 \cdot 10^0$	$4.5 \cdot 10^0$	$7.6 \cdot 10^0$	$1.3 \cdot 10^1$	$2.1 \cdot 10^1$	$3.5 \cdot 10^1$	$5.7 \cdot 10^1$
128	$2.7 \cdot 10^0$	$4.5 \cdot 10^0$	$7.6 \cdot 10^0$	$1.3 \cdot 10^1$	$2.1 \cdot 10^1$	$3.5 \cdot 10^1$	$5.7 \cdot 10^1$
256	$2.7 \cdot 10^0$	$4.5 \cdot 10^0$	$7.6 \cdot 10^0$	$1.3 \cdot 10^1$	$2.1 \cdot 10^1$	$3.5 \cdot 10^1$	$5.7 \cdot 10^1$
512	$2.7 \cdot 10^0$	$4.5 \cdot 10^0$	$7.6 \cdot 10^0$	$1.3 \cdot 10^1$	$2.1 \cdot 10^1$	$3.5 \cdot 10^1$	$5.7 \cdot 10^1$
1024	$2.7 \cdot 10^0$	$4.5 \cdot 10^0$	$7.6 \cdot 10^0$	$1.3 \cdot 10^1$	$2.1 \cdot 10^1$	$3.5 \cdot 10^1$	$5.7 \cdot 10^1$

Table 1:  $\kappa_2(\mathbf{U}_i)$  for different polynomial degree  $p_s$  and number of dyadic subdivisions  $n_{sub}$ .

## 4.2 Stable factorization of the pencil $(\widehat{\mathbf{W}}_t, \widehat{\mathbf{M}}_t)$

### 4.2.1 Numerical instability of the eigendecomposition

While  $\widehat{\mathbf{M}}_t$  is symmetric,  $\widehat{\mathbf{W}}_t$  is neither symmetric nor skew-symmetric. Indeed

$$[\widehat{\mathbf{W}}_t]_{i,j} + [\widehat{\mathbf{W}}_t]_{j,i} = \int_0^1 \widehat{b}'_{j,p_t}(t) \widehat{b}_{i,p_t}(\tau) \, d\tau + \int_0^1 \widehat{b}'_{i,p_t}(\tau) \widehat{b}_{j,p_t}(\tau) \, d\tau = \widehat{b}_{i,p_t}(1) \widehat{b}_{j,p_t}(1) \quad (4.6)$$

where  $\widehat{b}_{i,p_t}(1) \widehat{b}_{j,p_t}(1)$  vanishes for all  $i = 1, \dots, n_t - 1$  or  $j = 1, \dots, n_t - 1$ . A numerical computation of the generalized eigendecomposition of the pencil  $(\widehat{\mathbf{W}}_t, \widehat{\mathbf{M}}_t)$ , that is

$$\widehat{\mathbf{W}}_t \mathbf{U} = \widehat{\mathbf{M}}_t \mathbf{U} \boldsymbol{\Lambda}_t, \quad (4.7)$$

where  $\boldsymbol{\Lambda}_t$  is the diagonal matrix of the generalized complex eigenvalues and  $\mathbf{U}$  is the complex matrix whose columns are the generalized eigenvectors (with normalization w.r.t. the  $\|\cdot\|_{\widehat{\mathbf{M}}_t}$ -norm), reveals that the eigenvectors are far from  $\widehat{\mathbf{M}}_t$ -orthogonality, i.e. the matrix  $\mathbf{U}^* \widehat{\mathbf{M}}_t \mathbf{U}$  is not diagonal. As seen in Table 2 and Table 3, the numerically computed condition numbers  $\kappa_2(\mathbf{U})$  and  $\kappa_{\widehat{\mathbf{M}}_t}(\mathbf{U})$  are large and grow exponentially with respect to the degree  $p_t$  and the level of mesh refinement, in contrast to the spatial case (see Table 1).

$n_{sub}$	$p_t = 2$	$p_t = 3$	$p_t = 4$	$p_t = 5$	$p_t = 6$	$p_t = 7$	$p_t = 8$
32	$8.9 \cdot 10^2$	$3.0 \cdot 10^4$	$5.0 \cdot 10^4$	$3.4 \cdot 10^5$	$3.1 \cdot 10^6$	$4.2 \cdot 10^7$	$7.0 \cdot 10^8$
64	$4.4 \cdot 10^3$	$2.6 \cdot 10^5$	$5.0 \cdot 10^5$	$5.4 \cdot 10^6$	$8.9 \cdot 10^7$	$3.1 \cdot 10^9$	$2.0 \cdot 10^{10}$
128	$2.3 \cdot 10^4$	$1.2 \cdot 10^6$	$5.8 \cdot 10^6$	$1.0 \cdot 10^8$	$3.0 \cdot 10^9$	$6.4 \cdot 10^{11}$	$1.3 \cdot 10^{12}$
256	$1.2 \cdot 10^5$	$9.4 \cdot 10^6$	$7.6 \cdot 10^7$	$2.1 \cdot 10^9$	$1.2 \cdot 10^{11}$	$1.2 \cdot 10^{13}$	$2.1 \cdot 10^{13}$
512	$7.0 \cdot 10^5$	$8.3 \cdot 10^7$	$1.1 \cdot 10^9$	$4.9 \cdot 10^{10}$	$4.5 \cdot 10^{12}$	$3.6 \cdot 10^{13}$	$4.9 \cdot 10^{12}$
1024	$4.1 \cdot 10^6$	$8.0 \cdot 10^8$	$1.9 \cdot 10^{10}$	$1.3 \cdot 10^{12}$	$9.6 \cdot 10^{12}$	$1.4 \cdot 10^{12}$	$5.6 \cdot 10^{12}$

Table 2:  $\kappa_2(\mathbf{U})$  for different degree  $p_t$  and number of dyadic subdivisions  $n_{sub}$ .

$n_{sub}$	$p_t = 2$	$p_t = 3$	$p_t = 4$	$p_t = 5$	$p_t = 6$	$p_t = 7$	$p_t = 8$
32	$1.8 \cdot 10^3$	$7.7 \cdot 10^4$	$1.3 \cdot 10^5$	$6.3 \cdot 10^5$	$4.1 \cdot 10^6$	$3.6 \cdot 10^7$	$4.3 \cdot 10^8$
64	$9.9 \cdot 10^3$	$7.9 \cdot 10^5$	$1.5 \cdot 10^6$	$1.3 \cdot 10^7$	$1.5 \cdot 10^8$	$3.6 \cdot 10^9$	$1.4 \cdot 10^{10}$
128	$5.5 \cdot 10^4$	$4.0 \cdot 10^6$	$2.1 \cdot 10^7$	$3.1 \cdot 10^8$	$6.8 \cdot 10^9$	$1.1 \cdot 10^{12}$	$1.1 \cdot 10^{12}$
256	$3.2 \cdot 10^5$	$3.3 \cdot 10^7$	$3.3 \cdot 10^8$	$8.6 \cdot 10^9$	$3.5 \cdot 10^{11}$	$2.3 \cdot 10^{13}$	$2.8 \cdot 10^{13}$
512	$1.8 \cdot 10^6$	$3.1 \cdot 10^8$	$5.6 \cdot 10^9$	$2.5 \cdot 10^{11}$	$1.9 \cdot 10^{13}$	$1.6 \cdot 10^{14}$	$9.3 \cdot 10^{12}$
1024	$1.1 \cdot 10^7$	$3.1 \cdot 10^9$	$1.0 \cdot 10^{11}$	$8.6 \cdot 10^{12}$	$5.6 \cdot 10^{13}$	$6.0 \cdot 10^{12}$	$6.1 \cdot 10^{12}$

Table 3:  $\kappa_{\widehat{\mathbf{M}}_t}(\mathbf{U})$  for different degree  $p_t$  and number of dyadic subdivisions  $n_{sub}$ .

These tests clearly indicate a numerical instability when computing the generalized eigendecomposition of  $(\widehat{\mathbf{W}}_t, \widehat{\mathbf{M}}_t)$ . Similar instabilities have also been highlighted in [14].

#### 4.2.2 Construction of the stable factorization

The analysis above motivates the search of a different but stable factorization of the pencil  $(\widehat{\mathbf{W}}_t, \widehat{\mathbf{M}}_t)$ . We look now for a factorization of the form

$$\widehat{\mathbf{W}}_t \mathbf{U}_t = \widehat{\mathbf{M}}_t \mathbf{U}_t \Delta_t, \quad (4.8)$$

where  $\Delta_t$  is a complex matrix with non-zero entries allowed on the diagonal, on the last row and on the last column only. We also require that  $\mathbf{U}_t$  fulfils the orthogonality condition

$$\mathbf{U}_t^* \widehat{\mathbf{M}}_t \mathbf{U}_t = \mathbb{I}_{n_t}. \quad (4.9)$$

From (4.8)–(4.9) we then obtain the factorizations

$$\mathbf{U}_t^* \widehat{\mathbf{W}}_t \mathbf{U}_t = \Delta_t \quad \text{and} \quad \mathbf{U}_t^* \widehat{\mathbf{M}}_t \mathbf{U}_t = \mathbb{I}_{n_t}. \quad (4.10)$$

With this aim, we look for  $\mathbf{U}_t$  as follows:

$$\mathbf{U}_t := \begin{bmatrix} \mathring{\mathbf{U}}_t & \mathbf{r} \\ \mathbf{0}^T & \rho \end{bmatrix} \quad (4.11)$$

where  $\mathring{\mathbf{U}}_t \in \mathbb{C}^{(n_t-1) \times (n_t-1)}$ ,  $\mathbf{r} \in \mathbb{C}^{n_t-1}$ ,  $\rho \in \mathbb{C}$  and where  $\mathbf{0} \in \mathbb{R}^{n_t-1}$  denotes the null vector. In order to guarantee the non-singularity of  $\mathbf{U}_t$ , we further impose  $\rho \neq 0$ . Accordingly, we split the time matrices  $\widehat{\mathbf{W}}_t$  and  $\widehat{\mathbf{M}}_t$  as

$$\widehat{\mathbf{W}}_t = \begin{bmatrix} \mathring{\mathbf{W}}_t & \mathbf{w} \\ -\mathbf{w}^T & \omega \end{bmatrix} \quad \text{and} \quad \widehat{\mathbf{M}}_t = \begin{bmatrix} \mathring{\mathbf{M}}_t & \mathbf{m} \\ \mathbf{m}^T & \mu \end{bmatrix}, \quad (4.12)$$

where we have defined

$$\begin{aligned} \omega &:= [\widehat{\mathbf{W}}_t]_{n_t, n_t}, & \mu &:= [\widehat{\mathbf{M}}_t]_{n_t, n_t}, \\ [\mathbf{w}]_i &= [\widehat{\mathbf{W}}_t]_{i, n_t} \quad \text{and} \quad [\mathbf{m}]_i = [\widehat{\mathbf{M}}_t]_{i, n_t} \quad \text{for } i = 1, \dots, n_t - 1, \\ [\mathring{\mathbf{W}}_t]_{i, j} &= [\widehat{\mathbf{W}}_t]_{i, j} \quad \text{and} \quad [\mathring{\mathbf{M}}_t]_{i, j} = [\widehat{\mathbf{M}}_t]_{i, j} \quad \text{for } i, j = 1, \dots, n_t - 1. \end{aligned} \quad (4.13)$$

Recalling (4.6), we observe that  $\mathring{\mathbf{W}}_t$  is skew-symmetric and, since  $\mathring{\mathbf{M}}_t$  is symmetric, we can write the eigendecomposition of the pencils  $(\mathring{\mathbf{W}}_t, \mathring{\mathbf{M}}_t)$ :

$$\mathring{\mathbf{W}}_t \mathring{\mathbf{U}}_t = \mathring{\mathbf{M}}_t \mathring{\mathbf{U}}_t \mathring{\Lambda}_t \quad \text{with} \quad \mathring{\mathbf{U}}_t^* \mathring{\mathbf{M}}_t \mathring{\mathbf{U}}_t = \mathbb{I}_{n_t-1}, \quad (4.14)$$

where  $\mathring{\mathbf{U}}_t$  contains the complex generalized eigenvectors and  $\mathring{\Lambda}_t$  is the diagonal matrix of the generalized eigenvalues, that are pairs of complex conjugate pure imaginary numbers plus, eventually, the eigenvalue zero. From (4.11)–(4.12), it follows

$$\mathbf{U}_t^* \widehat{\mathbf{M}}_t \mathbf{U}_t = \begin{bmatrix} \mathbb{I}_{n_t-1} & \mathring{\mathbf{U}}_t^* \mathring{\mathbf{M}}_t \mathbf{r} + \mathring{\mathbf{U}}_t^* \mathbf{m} \rho \\ \mathbf{r}^* \mathring{\mathbf{M}}_t \mathring{\mathbf{U}}_t + \rho^* \mathbf{m}^T \mathring{\mathbf{U}}_t & [\mathbf{r}^* \rho^*] \widehat{\mathbf{M}}_t \begin{bmatrix} \mathbf{r} \\ \rho \end{bmatrix} \end{bmatrix},$$

where for the top-left block we have used (4.14).

The orthogonality condition in (4.9) holds if and only if  $\mathbf{r}$  and  $\rho$  fulfil the two conditions:

$$\begin{cases} \mathring{\mathbf{U}}_t^* \mathring{\mathbf{M}}_t \mathbf{r} + \mathring{\mathbf{U}}_t^* \mathbf{m} \rho = \mathbf{0}, \end{cases} \quad (4.15a)$$

$$\begin{cases} [\mathbf{r}^* \rho^*] \widehat{\mathbf{M}}_t \begin{bmatrix} \mathbf{r} \\ \rho \end{bmatrix} = 1. \end{cases} \quad (4.15b)$$

In order to calculate  $\mathbf{r}$  and  $\rho$ , we first find  $\mathbf{v} \in \mathbb{C}^{n_t-1}$  such that

$$\mathring{\mathbf{M}}_t \mathbf{v} = -\mathbf{m}; \quad (4.16)$$

then normalize the vector  $\begin{bmatrix} \mathbf{v} \\ 1 \end{bmatrix}$  w.r.t. the  $\|\cdot\|_{\widehat{\mathbf{M}}_t}$ -norm to get

$$\begin{bmatrix} \mathbf{r} \\ \rho \end{bmatrix} := \frac{\begin{bmatrix} \mathbf{v} \\ 1 \end{bmatrix}}{\left( [\mathbf{v}^* \ 1] \widehat{\mathbf{M}}_t \begin{bmatrix} \mathbf{v} \\ 1 \end{bmatrix} \right)^{\frac{1}{2}}}$$

that fulfils (4.15a)–(4.15b). Finally, we get (4.8) by defining

$$\Delta_t := \mathbf{U}_t^* \widehat{\mathbf{W}}_t \mathbf{U}_t = \begin{bmatrix} \mathring{\Lambda}_t & \mathbf{l} \\ -\mathbf{l}^* & \sigma \end{bmatrix}, \quad (4.17)$$

where  $\mathbf{l} := \mathring{\mathbf{U}}_t^* \begin{bmatrix} \mathring{\mathbf{W}}_t \ \mathbf{w} \\ \rho \end{bmatrix} \begin{bmatrix} \mathbf{r} \\ \rho \end{bmatrix}$  and  $\sigma := [\mathbf{r}^* \rho^*] \widehat{\mathbf{W}}_t \begin{bmatrix} \mathbf{r} \\ \rho \end{bmatrix}$ . Note that matrix (4.17) has an arrowhead structure.

To assess the stability of the new decomposition (4.10), we compute the condition numbers  $\kappa_2(\mathbf{U}_t)$  for dyadically refined uniform knot spans and different degrees. Thanks to (4.9), we have  $\kappa_2(\mathbf{U}_t) = \sqrt{\kappa_2(\widehat{\mathbf{M}}_t)}$ . The results, reported in Table 4, show that the condition numbers  $\kappa_2(\mathbf{U}_t)$  are uniformly bounded w.r.t. the mesh refinement, they grow with respect to the polynomial degree but they are moderately small for all the degrees of interest. As a consequence of (4.9), we also have that  $\kappa_{\widehat{\mathbf{M}}_t}(\mathbf{U}_t) = 1$ . We conclude that the factorization (4.10) for the time pencil  $(\widehat{\mathbf{W}}_t, \widehat{\mathbf{M}}_t)$  is stable.

### 4.3 Preconditioner application

The application of the preconditioner involves the solution of the linear system

$$\widehat{\mathbf{A}} \mathbf{s} = \mathbf{r}, \quad (4.18)$$

where  $\widehat{\mathbf{A}}$  has the structure (4.1). We are able to efficiently solve system (4.18) by extending the fast diagonalization method. The starting points, that are involved in the setup of the preconditioner, are the following ones:

$n_{sub}$	$p_t = 2$	$p_t = 3$	$p_t = 4$	$p_t = 5$	$p_t = 6$	$p_s = 7$	$p_s = 8$
32	$3.2 \cdot 10^0$	$5.2 \cdot 10^0$	$8.3 \cdot 10^0$	$1.3 \cdot 10^1$	$2.2 \cdot 10^1$	$3.6 \cdot 10^1$	$5.9 \cdot 10^1$
64	$3.3 \cdot 10^0$	$5.2 \cdot 10^0$	$8.3 \cdot 10^0$	$1.3 \cdot 10^1$	$2.2 \cdot 10^1$	$3.6 \cdot 10^1$	$5.9 \cdot 10^1$
128	$3.3 \cdot 10^0$	$5.2 \cdot 10^0$	$8.3 \cdot 10^0$	$1.3 \cdot 10^1$	$2.2 \cdot 10^1$	$3.6 \cdot 10^1$	$5.9 \cdot 10^1$
256	$3.3 \cdot 10^0$	$5.2 \cdot 10^0$	$8.3 \cdot 10^0$	$1.3 \cdot 10^1$	$2.2 \cdot 10^1$	$3.6 \cdot 10^1$	$5.9 \cdot 10^1$
512	$3.3 \cdot 10^0$	$5.2 \cdot 10^0$	$8.3 \cdot 10^0$	$1.3 \cdot 10^1$	$2.2 \cdot 10^1$	$3.6 \cdot 10^1$	$5.9 \cdot 10^1$
1024	$3.3 \cdot 10^0$	$5.2 \cdot 10^0$	$8.3 \cdot 10^0$	$1.3 \cdot 10^1$	$2.2 \cdot 10^1$	$3.6 \cdot 10^1$	$5.9 \cdot 10^1$

Table 4:  $\kappa_2(\mathbf{U}_t)$  for different degree  $p_t$  and number of dyadic subdivisions  $n_{sub}$ .

- for the pencils  $(\widehat{\mathbf{K}}_i, \widehat{\mathbf{M}}_i)$  for  $i = 1, \dots, d$  we have the factorizations (4.5);
- for the pencil  $(\widehat{\mathbf{W}}_t, \widehat{\mathbf{M}}_t)$  we have the factorization (4.10).

Then, by defining  $\mathbf{U}_s := \mathbf{U}_d \otimes \dots \otimes \mathbf{U}_1$  and  $\Lambda_s := \sum_{i=1}^d \mathbb{I}_{n_{s,d}} \otimes \dots \otimes \mathbb{I}_{n_{s,i+1}} \otimes \Lambda_i \otimes \mathbb{I}_{n_{s,i-1}} \otimes \dots \otimes \mathbb{I}_{n_{s,1}}$ , we have for the matrix  $\widehat{\mathbf{A}}$  the factorization

$$\widehat{\mathbf{A}} = (\mathbf{U}_t^* \otimes \mathbf{U}_s^T)^{-1} (\gamma \Delta_t \otimes \mathbb{I}_{N_s} + \nu \mathbb{I}_{n_t} \otimes \Lambda_s) (\mathbf{U}_t \otimes \mathbf{U}_s)^{-1}. \quad (4.19)$$

Note that the second factor in (4.19) has the block-arrowhead structure

$$\gamma \Delta_t \otimes \mathbb{I}_{N_s} + \nu \mathbb{I}_{n_t} \otimes \Lambda_s = \begin{bmatrix} \mathbf{H}_1 & & \mathbf{B}_1 \\ & \ddots & \vdots \\ & & \mathbf{H}_{n_t-1} & \mathbf{B}_{n_t-1} \\ -\mathbf{B}_1^* & \dots & -\mathbf{B}_{n_t-1}^* & \mathbf{H}_{n_t} \end{bmatrix} \quad (4.20)$$

where  $\mathbf{H}_i$  and  $\mathbf{B}_i$  are diagonal matrices defined as

$$\mathbf{H}_i := \gamma [\Lambda_t]_{ii} \mathbb{I}_{N_s} + \nu \Lambda_s \quad \text{and} \quad \mathbf{B}_i := \gamma [\mathbf{l}]_i \mathbb{I}_{N_s} \quad \text{for} \quad i = 1, \dots, n_t - 1,$$

$$\mathbf{H}_{n_t} := \gamma \sigma \mathbb{I}_{N_s} + \nu \Lambda_s.$$

The matrix (4.20) has the following easy-to-invert block LU decomposition

$$\gamma \Delta_t \otimes \mathbb{I}_{N_s} + \nu \mathbb{I}_{n_t} \otimes \Lambda_s = \begin{bmatrix} \mathbb{I}_{N_s} & & & & \mathbf{H}_1 & & \mathbf{B}_1 \\ & \ddots & & & & \vdots & \\ & & \mathbb{I}_{N_s} & & & & \\ -\mathbf{B}_1^* \mathbf{H}_1^{-1} & \dots & -\mathbf{B}_{n_t-1}^* \mathbf{H}_{n_t-1}^{-1} & \mathbb{I}_{N_s} & & \mathbf{H}_{n_t-1} & \mathbf{B}_{n_t-1} \\ \end{bmatrix} \begin{bmatrix} & & & & \mathbf{H}_1 & & \mathbf{B}_1 \\ & & & & & \vdots & \\ & & & & & & \\ & & & & & \mathbf{H}_{n_t-1} & \mathbf{B}_{n_t-1} \\ & & & & & & \mathbf{S} \end{bmatrix} \quad (4.21)$$

where  $\mathbf{S} := \mathbf{H}_{n_t} + \sum_{i=1}^{n_t-1} \mathbf{B}_i^* \mathbf{H}_i^{-1} \mathbf{B}_i$  is a diagonal matrix.

Summarising, the solution of (4.18) can be computed by the following algorithm.

---

**Algorithm 1** Extended FD

---

- 1: Compute the factorizations (4.5) and (4.10).
- 2: Compute  $\tilde{\mathbf{s}} = (\mathbf{U}_t^* \otimes \mathbf{U}_s^T) \mathbf{s}$ .
- 3: Compute  $\tilde{\mathbf{q}} = (\gamma \Delta_t \otimes \mathbb{I}_{N_s} + \nu \mathbb{I}_{n_t} \otimes \Lambda_s)^{-1} \tilde{\mathbf{s}}$ .
- 4: Compute  $\mathbf{r} = (\mathbf{U}_t \otimes \mathbf{U}_s) \tilde{\mathbf{q}}$ .

---

#### 4.4 Preconditioner robustness: partial inclusion of the geometry

The preconditioner (4.1) does not incorporate any information on the geometry parametrization  $\mathbf{G}$ . Thus, the performance of  $\widehat{\mathbf{A}}$  may depend on the geometry map: we see this trend in the numerical tests of Section 5 and, in particular, in the upper tables of Table 5 and Table 7. However, we can generalize (4.1) by including in the time matrices  $\widehat{\mathbf{W}}_t$  and  $\widehat{\mathbf{M}}_t$  and in the univariate spatial matrices  $\widehat{\mathbf{K}}_i, \widehat{\mathbf{M}}_i$  for  $i = 1, \dots, d$  a suitable approximation of

$\mathbf{G}$ , without increasing the asymptotic computational cost. A similar approach has been used also in [22] for the Stokes problem and in [21] for a least-squares formulation of the heat equation. We briefly give an overview of this strategy.

Referring to Section 2.2 for the notation of the basis functions, we rewrite the entries of the system matrix (3.5) in the parametric domain as

$$\begin{aligned} [\mathbf{A}]_{i,j} &= \mathcal{A}(B_{j,\mathbf{p}}, B_{i,\mathbf{p}}) \\ &= \gamma \int_0^1 \int_{\widehat{\Omega}} \frac{1}{T} \partial_\tau \widehat{B}_{j,\mathbf{p}} \widehat{B}_{i,\mathbf{p}} |\det(J_{\mathbf{G}})| d\widehat{\Omega} d\tau + \int_0^1 \int_{\widehat{\Omega}} \nu (\nabla \widehat{B}_{j,\mathbf{p}})^T J_{\mathbf{G}}^{-1} J_{\mathbf{G}}^{-T} \nabla \widehat{B}_{i,\mathbf{p}} |\det(J_{\mathbf{G}})| d\widehat{\Omega} d\tau \\ &= \int_0^1 \int_{\widehat{\Omega}} \begin{bmatrix} (\nabla \widehat{B}_{j,\mathbf{p}})^T & \partial_\tau \widehat{B}_{j,\mathbf{p}} \end{bmatrix} \mathfrak{C} \begin{bmatrix} (\nabla \widehat{B}_{i,\mathbf{p}})^T & \widehat{B}_{i,\mathbf{p}} \end{bmatrix}^T d\widehat{\Omega} d\tau, \end{aligned} \quad (4.22)$$

where

$$\mathfrak{C} := \begin{bmatrix} \nu J_{\mathbf{F}}^{-1} J_{\mathbf{F}}^{-T} |\det(J_{\mathbf{F}})| T & \\ & \gamma |\det(J_{\mathbf{F}})| \end{bmatrix}$$

and where we used that  $B_{i,\mathbf{p}} = \widehat{B}_{i,\mathbf{p}} \circ \mathbf{G}^{-1}$ ,  $B_{j,\mathbf{p}} = \widehat{B}_{j,\mathbf{p}} \circ \mathbf{G}^{-1}$  and  $|\det(J_{\mathbf{G}})| = T |\det(J_{\mathbf{F}})|$ . The construction of the preconditioner is based on the following approximation of the diagonal entries only of  $\mathfrak{C}$ :

$$[\mathfrak{C}(\boldsymbol{\eta}, \tau)]_{k,k} \approx [\widetilde{\mathfrak{C}}(\boldsymbol{\eta}, \tau)]_{k,k} := \varphi_1(\eta_1) \dots \varphi_{k-1}(\eta_{k-1}) \Phi_k(\eta_k) \varphi_{k+1}(\eta_{k+1}) \dots \varphi_d(\eta_d) \varphi_{d+1}(\tau) \quad k = 1, \dots, d, \quad (4.23a)$$

$$[\mathfrak{C}(\boldsymbol{\eta}, \tau)]_{d+1,d+1} \approx [\widetilde{\mathfrak{C}}(\boldsymbol{\eta}, \tau)]_{d+1,d+1} := \varphi_1(\eta_1) \dots \varphi_d(\eta_d) \Phi_{d+1}(\tau). \quad (4.23b)$$

We interpolate the functions  $\widetilde{\mathfrak{C}}_{k,k}$  in (4.23) by piecewise constants in each element and we build the univariate factors  $\varphi_k$  and  $\Phi_k$  by using the separation of variables algorithm detailed in [21, Appendix C]. The computational cost of the approximation above is proportional to the number of elements, that, when using smooth B-splines, is almost equal to  $N_{dof}$  and it is independent of  $p_s$  and  $p_t$  and thus negligible in the whole iterative strategy.

Then we define

$$[\widetilde{\mathbf{A}}]_{i,j} := \int_0^1 \int_{\widehat{\Omega}} \begin{bmatrix} (\nabla \widehat{B}_{j,\mathbf{p}})^T & \partial_\tau \widehat{B}_{j,\mathbf{p}} \end{bmatrix} \widetilde{\mathfrak{C}} \begin{bmatrix} (\nabla \widehat{B}_{i,\mathbf{p}})^T & \widehat{B}_{i,\mathbf{p}} \end{bmatrix}^T d\widehat{\Omega} d\tau.$$

The previous matrix maintains the same Kronecker structure as (4.1):

$$\widetilde{\mathbf{A}} = \widetilde{\mathbf{W}}_t \otimes \widetilde{\mathbf{M}}_s + \widetilde{\mathbf{M}}_t \otimes \widetilde{\mathbf{K}}_s, \quad (4.24)$$

where

$$\begin{aligned} [\widetilde{\mathbf{W}}_t]_{i,j} &:= \int_0^1 \Phi_{d+1}(\tau) \widehat{b}'_{j,p_t}(\tau) \widehat{b}_{i,p_t}(\tau) d\tau \quad \text{and} \quad [\widetilde{\mathbf{M}}_t]_{i,j} := \int_0^1 \varphi_{d+1}(\tau) \widehat{b}_{i,p_t}(\tau) \widehat{b}_{j,p_t}(\tau) d\tau \quad \text{for } i, j = 1, \dots, n_t, \\ \widetilde{\mathbf{K}}_s &:= \sum_{k=1}^d \widetilde{\mathbf{M}}_d \otimes \dots \otimes \widetilde{\mathbf{M}}_{k+1} \otimes \widetilde{\mathbf{K}}_k \otimes \widetilde{\mathbf{M}}_{k-1} \otimes \dots \otimes \widetilde{\mathbf{M}}_1, \quad \widetilde{\mathbf{M}}_s := \widetilde{\mathbf{M}}_d \otimes \dots \otimes \widetilde{\mathbf{M}}_1, \end{aligned}$$

and where for  $k = 1, \dots, d$  and for  $i, j = 1, \dots, n_{s,k}$  we define

$$[\widetilde{\mathbf{K}}_k]_{i,j} := \int_0^1 \Phi_k(\eta_k) \widehat{b}'_{i,p_s}(\eta_k) \widehat{b}'_{j,p_s}(\eta_k) d\eta_k \quad \text{and} \quad [\widetilde{\mathbf{M}}_k]_{i,j} := \int_0^1 \varphi_k(\eta_k) \widehat{b}_{i,p_s}(\eta_k) \widehat{b}_{j,p_s}(\eta_k) d\eta_k.$$

We remark that the application of (4.24) can still be performed by Algorithm 1. Finally, we apply a diagonal scaling on  $\widetilde{\mathbf{A}}$  and we define the preconditioner as

$$\widehat{\mathbf{A}}^{\mathbf{G}} := \mathbf{D}^{\frac{1}{2}} \widetilde{\mathbf{A}} \mathbf{D}^{\frac{1}{2}} \quad (4.25)$$

where  $[\mathbf{D}]_{i,i} := [\mathbf{A}]_{i,i} / [\widetilde{\mathbf{A}}]_{i,i}$ .

**Remark 2.** We remark that when  $\gamma$  and  $\nu$  do not depend on time, it holds

$$\mathbf{W}_t = \widehat{\mathbf{W}}_t \quad \text{and} \quad \mathbf{M}_t = T \widehat{\mathbf{M}}_t$$

and we can set explicitly  $\widetilde{\mathbf{W}}_t = \mathbf{W}_t$  and  $\widetilde{\mathbf{M}}_t = \mathbf{M}_t$ . However, as in our numerical tests we consider a more general framework in which  $\gamma$  and  $\nu$  depend on time, we have presented the more general strategy above, that allows to incorporate in  $\widehat{\mathbf{A}}^{\mathbf{G}}$  possible non-constant coefficients.

## 4.5 Computational cost and memory requirement

The linear system (3.5) is neither positive definite nor symmetric, and we choose GMRES as linear solver. In GMRES, the orthogonalization of the basis of the Krylov subspace makes the computational cost nonlinear with respect to the number of iterations. However, as long as this number is not too high, at each iteration the two dominant costs are the application of the preconditioning strategy and the computation of the residual. We assume, for simplicity that for  $i = 1, \dots, d$  the matrices  $\widehat{\mathbf{K}}_i, \widehat{\mathbf{M}}_i$  and  $\widetilde{\mathbf{K}}_i, \widetilde{\mathbf{M}}_i$  have dimensions  $n_s \times n_s$  and that the matrices  $\widehat{\mathbf{W}}_t, \widehat{\mathbf{M}}_t$  and  $\widetilde{\mathbf{W}}_t, \widetilde{\mathbf{M}}_t$  have dimensions  $n_t \times n_t$ . Thus the total number of degrees-of-freedom is  $N_{dof} = N_s n_t = n_s^d n_t$ .

The setup of  $\widehat{\mathbf{A}}$  and  $\widehat{\mathbf{A}}^G$  includes the operations performed in Step 1 of Algorithm 1, i.e.  $d$  spatial eigen-decompositions, that have a total cost of  $O(dn_s^3)$  FLOPs, and the factorization of the time matrices. The computational cost of the latter is the sum of the cost of the eigendecomposition (4.14) and of the cost of the solution of the linear system (4.16), yielding a cost of  $O(n_t^3)$  FLOPs. Then, the total cost of the space and time factorizations is  $O(dn_s^3 + n_t^3)$  FLOPs. Note that, if  $n_t = O(n_s)$ , this cost is optimal for  $d = 2$  and negligible for  $d = 3$ . The setup cost of  $\widehat{\mathbf{A}}^G$  includes also the construction of the diagonal matrix  $\mathbf{D}$ , that has a negligible cost, and the computation of the  $2(d+1)$  approximations  $\varphi_1, \dots, \varphi_{d+1}$  and  $\Phi_1, \dots, \Phi_{d+1}$  in (4.23), that, as mentioned in Section 4.4, has the optimal cost of  $O(N_{dof})$  FLOPs. We remark that the setup of the preconditioners has to be performed only once, since the matrices involved do not change during the iterative procedure.

The application of the preconditioner is performed by Steps 2-4 of Algorithm 1. Exploiting (2.5), Step 2 and Step 4 costs  $4(dn_s^{d+1} n_t + n_t^2 n_s^d) = 4N_{dof}(dn_s + n_t)$  FLOPs. The use of the block LU decomposition (4.21) makes the cost for Step 3 equal to  $O(N_{dof})$  FLOPs.

In conclusion, the total cost of Algorithm 1 is  $4N_{dof}(dn_s + n_t) + O(N_{dof})$  FLOPs. The non-optimal dominant cost of Step 2 and Step 4 is determined by the dense matrix-matrix products. However, these operations are usually implemented on modern computers in a very efficient way. For this reason, in our numerical tests, the overall serial computational time grows almost as  $O(N_{dof})$ , see Figure 3 in Section 5.

The other dominant computational cost in a GMRES iteration is the cost of the residual computation, that is the multiplication of the matrix  $\mathbf{A}$  with a vector. This multiplication is done by exploiting the special structure (3.6), that allows a matrix-free approach and the use of formula (2.5). Note in particular that we do not need to compute and to store the whole matrix  $\mathbf{A}$ , but only its time and spatial factors. Since the time matrices  $\mathbf{M}_t$  and  $\mathbf{W}_t$  are banded with a band of width  $2p_t + 1$  and the spatial matrices  $\mathbf{K}_s$  and  $\mathbf{M}_s$  have roughly  $N_s(2p_s + 1)^d$  nonzero entries, we have that the computational cost of a single matrix-vector product is  $6N_{dof}[(2p_s + 1)^d + 2p_t + 1] \approx 6N_{dof}(2p + 1)^d = O(N_{dof}p^d)$  FLOPs, if we assume  $p = p_s \approx p_t$ . The numerical experiments reported in Table 6 of Section 5 show that the dominant cost in the iterative solver is represented by the residual computation. This is a typical behaviour of the FD-based preconditioning strategies, see [21, 22, 24].

We now investigate the memory consumption. For the preconditioner we have to store the eigenvector spatial matrices  $\mathbf{U}_1, \dots, \mathbf{U}_d$ , the time matrix  $\mathbf{U}_t$  and the block-arrowhead matrix (4.20). The memory required is roughly

$$n_t^2 + dn_s^2 + 2N_{dof}.$$

For the system matrix, we have to store the time factors  $\mathbf{M}_t$  and  $\mathbf{W}_t$  and the spatial factors  $\mathbf{M}_s$  and  $\mathbf{K}_s$ . Thus the memory required is roughly

$$2(2p_t + 1)n_t + 2(2p_s + 1)^d N_s \approx 4p_t n_t + 2^{d+1} p_s^d N_s.$$

As for the least-squares case [21], we conclude that, in terms of memory requirement, our approach is very attractive w.r.t. other approaches, e.g. the ones obtained by discretizing in space and in time separately. For example if we assume  $d = 3$ ,  $p_t \approx p_s = p$  and  $n_t^2 \leq Cp^3 N_s$ , then the total memory consumption is  $O(p^3 N_s + N_{dof})$ , that is equal to the sum of the memory needed to store the Galerkin matrices associated to spatial variables and the memory needed to store the solution of the problem.

We remark that we could avoid storing the factors of  $\mathbf{A}$  by using the matrix-free approach of [25]. The memory and the computational cost of the iterative solver would significantly improve, both for the setup and the matrix-vector multiplications. However, we do not pursue this strategy, as it is beyond the scope of this paper.

**Remark 3.** *For a better computational efficiency, we use a real-arithmetic version of Algorithm 1: we replace  $\widetilde{\mathbf{A}}_t$  in (4.17) by a block diagonal matrix where each pair of generalized eigenvalues  $i\lambda_j$  and  $-i\lambda_j$  is replaced by*

a diagonal block

$$\begin{bmatrix} 0 & \lambda_j \\ -\lambda_j & 0 \end{bmatrix}$$

and we set

$$\mathbf{H}_j := \begin{bmatrix} \nu \mathbf{\Lambda}_s & \gamma \lambda_j \mathbb{I}_{n_s} \\ -\gamma \lambda_j \mathbb{I}_{n_s} & \nu \mathbf{\Lambda}_s \end{bmatrix} \quad \text{and} \quad \mathbf{B}_j := \gamma \begin{bmatrix} [\mathbf{l}]_{2(j-1)+1} \mathbb{I}_{N_s}, & [\mathbf{l}]_{2(j-1)+2} \mathbb{I}_{N_s} \end{bmatrix}^T.$$

Note that the computational cost of Step 3 in Algorithm 1 does not change, as we have

$$\mathbf{H}_j^{-1} := \begin{bmatrix} \frac{1}{\nu} \mathbf{\Lambda}_s^{-1} - \frac{\gamma^2}{\nu^2} \lambda_j^2 \mathbf{\Lambda}_s^{-1} \left( \nu \mathbf{\Lambda}_s + \frac{\gamma^2}{\nu} \lambda_j^2 \mathbf{\Lambda}_s^{-1} \right)^{-1} \mathbf{\Lambda}_s^{-1} & -\frac{\gamma}{\nu} \lambda_j \mathbf{\Lambda}_s^{-1} \left( \nu \mathbf{\Lambda}_s + \frac{\gamma^2}{\nu} \lambda_j^2 \mathbf{\Lambda}_s^{-1} \right)^{-1} \\ \frac{\gamma}{\nu} \lambda_j \left( \nu \mathbf{\Lambda}_s + \frac{\gamma^2}{\nu} \lambda_j^2 \mathbf{\Lambda}_s^{-1} \right)^{-1} \mathbf{\Lambda}_s^{-1} & \left( \nu \mathbf{\Lambda}_s + \frac{\gamma^2}{\nu} \lambda_j^2 \mathbf{\Lambda}_s^{-1} \right)^{-1} \end{bmatrix}.$$

## 5 Numerical Results

In this section we first present the numerical experiments that assess the convergence behavior of the Galerkin approximation and then we analyze the performance of the preconditioners. We also present a comparison with the the least-squares solver of [21].

We consider only sequential executions and we force the use of a single computational thread in a Intel Core i7-5820K processor, running at 3.30 GHz and with 64 GB of RAM.

The tests are performed with Matlab R2015a and GeoPDEs toolbox [33]. We use the `eig` Matlab function to compute the generalized eigendecompositions present in Step 1 of Algorithm 1, while Tensorlab toolbox [27] is employed to perform the multiplications with Kronecker matrices occurring in Step 2 and Step 4. The solution of the linear system (4.16) is performed by Matlab direct solver (backslash operator “\”).

The linear system is solved by GMRES without restart, with tolerance equal to  $10^{-8}$  and with the null vector as initial guess in all tests. We consider the same mesh-size in space and in time, by setting  $h_s = h_t =: h$ , and we denote the number of subdivisions in each parametric direction by  $n_{sub}$ . We use splines of maximal continuity allowed and of the same degree both in space and in time, i.e. we set  $p_t = p_s =: p$ . The symbol “\*” denotes that the construction of the matrix factors of  $\mathbf{A}$  (see (3.6)) goes out of memory, while the symbol “\*\*” indicates that the dimension of the Krylov subspace is too high and there is not enough memory to store all GMRES iterates. We remark that in all the tables the total solving time of the iterative strategies includes also the setup time of the considered preconditioner.

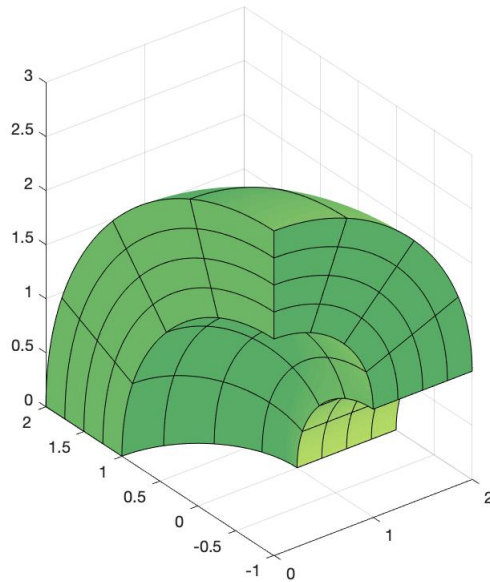
### 5.1 Orders of convergence

We consider as spatial computational domain  $\Omega$  a rotated quarter of annulus, represented in Figure 1a: we rotate by  $\frac{\pi}{2}$  a quarter of annulus with center in the origin, internal radius 1 and external radius 2 along the axis  $y = -1$ . Dirichlet and initial boundary conditions are set such that  $u(x, y, z, t) = -(x^2 + y^2 - 1)(x^2 + y^2 - 4)xy^2 \sin(t) \sin(z)$  is the exact solution with constants  $\nu = \gamma = 1$ .

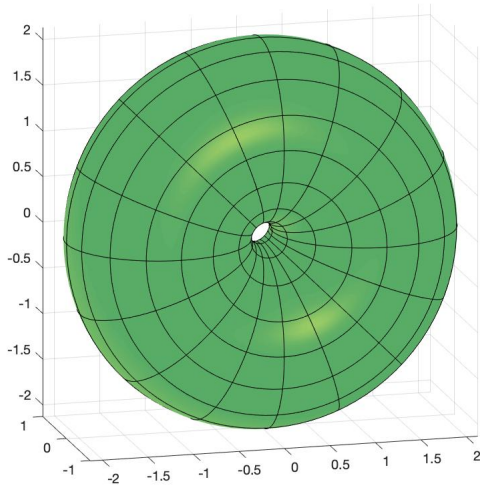
In Figure 2a we represent the relative errors in  $L^2(0, T; H_0^1(\Omega)) \cap H^1(0, T; L^2(\Omega))$  norm, an easily computable upper bound of  $\|\cdot\|_{\mathcal{X}_h}$ , for polynomial degrees  $p = 1, 2, 3, 4, 5$ . The rates of convergence are optimal, i.e. of order  $O(h^p)$ , consistent with the a-priori estimate (3.4). Even if this case is not covered by theoretical results, we also compute the relative errors in  $L^2(0, T; L^2(\Omega))$  norm: the orders of convergence are still optimal, that is of order  $O(h^{p+1})$ , as Figure 2b shows.

### 5.2 Performance of the preconditioner: rotated quarter of annulus

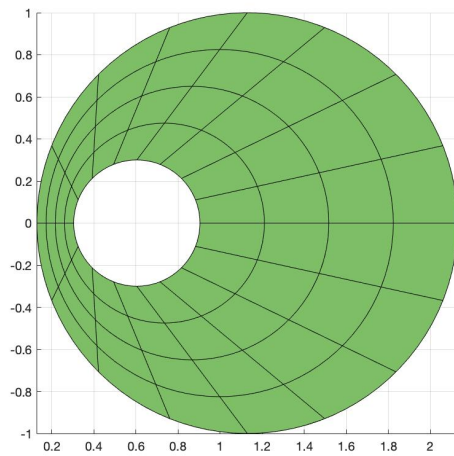
We consider again as spatial computational domain  $\Omega$  the rotated quarter of annulus of Figure 1a and the same exact solution, initial and boundary data as in Section 5.1. We analyze the performance of both  $\widehat{\mathbf{A}}$  and  $\widehat{\mathbf{A}}^G$ . The maximum dimension of the Krylov subspace is set equal to 100 for both the preconditioners up to  $n_{sub} = 64$ . We are able to reach convergence and to perform the tests with  $\widehat{\mathbf{A}}^G$ ,  $n_{sub} = 128$  and  $p = 1, 2, 3$  by setting the maximum Krylov subspace dimension equal to 25. In Table 5 we report the number of iterations and the total solving time of GMRES preconditioned with  $\widehat{\mathbf{A}}$  (upper table) and  $\widehat{\mathbf{A}}^G$  (middle table). The non-trivial geometry clearly affects the performance of  $\widehat{\mathbf{A}}$ , but, when we include some information on the parametrization by using  $\widehat{\mathbf{A}}^G$ , the number of iterations is more than halved and it is stable w.r.t.  $p$  and  $n_{sub}$ . Moreover, the computational times are one order of magnitude lower for the highest degrees and  $n_{sub}$ . In the lower table of Table 5 we report



(a) Rotated quarter of annulus.



(b) Hollow torus.



(c) Section of the hollow torus.

Figure 1: Computational domains.

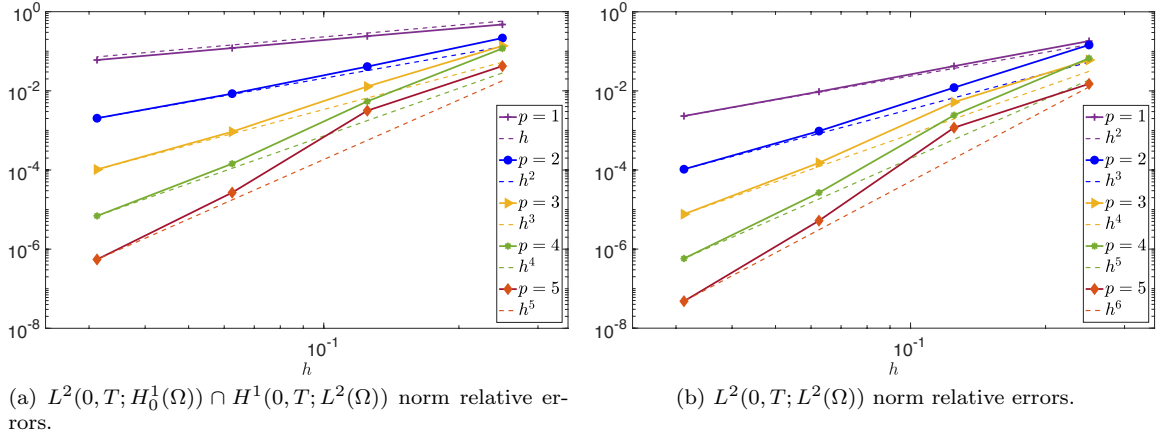


Figure 2: Relative errors.

the results of [21, Section 5] obtained by solving the same problem with the least-squares formulation and the related preconditioning strategy. In this case the iterative solver is the preconditioned conjugate gradient method, the tolerance is  $10^{-8}$  and the initial guess is the null vector. The number of iterations is more than doubled and the computational times are three times higher than the number of iterations and computational times of  $\widehat{\mathbf{A}}^G$ , in the present setting.

Finally, we analyze with more details the performance of  $\widehat{\mathbf{A}}^G$ . First, we consider the percentage of time spent in the application of  $\widehat{\mathbf{A}}^G$  in one GMRES iteration. The results, reported in Table 6, clearly show that the dominant cost consists of the matrix-vector multiplications, while the application of the preconditioner takes a small percentage of the total computational time, for example less than 10% for polynomial degree 5 and  $n_{sub} = 32$  or  $n_{sub} = 64$ . In Figure 3 we report the setup time and the single application time of  $\widehat{\mathbf{A}}^G$  w.r.t. the number of degrees of freedom. As expected, the setup time is proportional to  $O(N_{dof})$ . What is more interesting is that the application time grows slower than  $O(N_{dof}^{5/4})$ , i.e. the FLOPS counting, and it is almost proportional to  $O(N_{dof})$ : this may be explained by the fact that the memory access is the dominant cost due to the high-efficiency of CPU operations, in our case implemented in Matlab Tensorlab [27].

### 5.3 Performance of the preconditioner: hollow torus

We consider a torus with a hole (Figure 1b) that is obtained by revolving an eccentric annulus (Figure 1c) along the  $y$  axis. For this problem we consider  $\gamma = 1$  and a separable in space and time, non-constant diffusion coefficient  $\nu$ . Precisely, we choose

$$\nu(x, y, z, t) = \left\{ 1 + 50 \left[ 1 + \cos \left( \frac{t}{2\pi} \right) \right] \right\} \left\{ 1 + \frac{99}{2} \left[ 1 + \frac{1}{(1 + \frac{x^2}{z^2})^{\frac{1}{2}}} \right] \right\}.$$

The initial data and right-hand side are defined such that  $u(x, y, z, t) := \sin(\pi x) \sin(\pi y) \sin(\pi z) \sin(\pi t)$  is the exact solution. In this case, we replace  $\nu$  in (4.1) with its integral mean  $\frac{1}{T|\Omega|} \int_0^T \int_{\Omega} \nu(x, y, z, t) \, d\Omega \, dt$ . In Table 7 we compare the performance of  $\widehat{\mathbf{A}}$  (upper table) and  $\widehat{\mathbf{A}}^G$  (lower table): the inclusion of the information about the geometry parametrization and  $\nu$  significantly reduces the number of iterations and the computational times.

## 6 Conclusions

In this work we proposed a preconditioner suited for a space-time Galerkin isogeometric discretization of the heat equation. Our preconditioner  $\widehat{\mathbf{A}}$  is represented by a suitable sum of Kronecker products of matrices, that makes the computational cost of its construction (setup) and application, as well as the storage cost, very appealing. In particular the application of the preconditioner, inspired by the fast diagonalization technique,

	$\widehat{\mathbf{A}}$ Iterations / Time				
$n_{sub}$	$p = 1$	$p = 2$	$p = 3$	$p = 4$	$p = 5$
8	34 / 0.20	37 / 0.21	42 / 0.42	46 / 0.63	50 / 1.13
16	43 / 1.15	46 / 1.65	50 / 3.42	54 / 5.80	57 / 11.87
32	50 / 22.75	53 / 31.10	57 / 54.02	61 / 96.06	64 / 184.84
64	57 / 586.73	60 / 764.26	67 / 1254.81	67 / 1858.55	71 / 3188.51
128	**	**	**	*	*

	$\widehat{\mathbf{A}}^G$ Iterations / Time				
$n_{sub}$	$p = 1$	$p = 2$	$p = 3$	$p = 4$	$p = 5$
8	11 / 0.06	12 / 0.09	12 / 0.11	13 / 0.18	14 / 0.29
16	13 / 0.26	14 / 0.52	14 / 1.18	14 / 1.44	15 / 3.85
32	15 / 4.73	15 / 6.76	15 / 12.67	15 / 21.47	16 / 40.54
64	16 / 107.24	16 / 135.74	18 / 249.27	16 / 370.31	17 / 695.44
128	17 / 2623.57	17 / 3105.76	17 / 5614.10	*	*

	Least-squares Iterations / Time			
$n_{sub}$	$p_t = 2$	$p_t = 3$	$p_t = 4$	$p_t = 5$
8	24 / 0.09	24 / 0.13	26 / 0.37	26 / 0.60
16	35 / 0.77	34 / 1.96	33 / 4.62	33 / 9.35
32	42 / 17.03	41 / 39.57	40 / 82.35	41 / 161.73
64	46 / 333.20	44 / 716.03	49 / 1577.55	53 / 3384.08
128	48 / 6767.08	50 / 14814.09	*	*

Table 5: Revolved quarter domain. Performance of  $\widehat{\mathbf{A}}$ ,  $\widehat{\mathbf{A}}^G$  and the least-squares solver.

$n_{sub}$	$p = 1$	$p = 2$	$p = 3$	$p = 4$	$p = 5$
8	73.02 %	79.24 %	66.62 %	46.94 %	33.73 %
16	68.10 %	46.13 %	30.06 %	17.63 %	11.27 %
32	53.09 %	33.34 %	20.44 %	13.06 %	8.19 %
64	54.71 %	32.46 %	20.20 %	12.52 %	7.31 %
128	54.12 %	33.53 %	18.89 %	*	*

Table 6: Percentage of computing time of  $\widehat{\mathbf{A}}^G$  in one GMRES iteration for the rotated quarter domain.

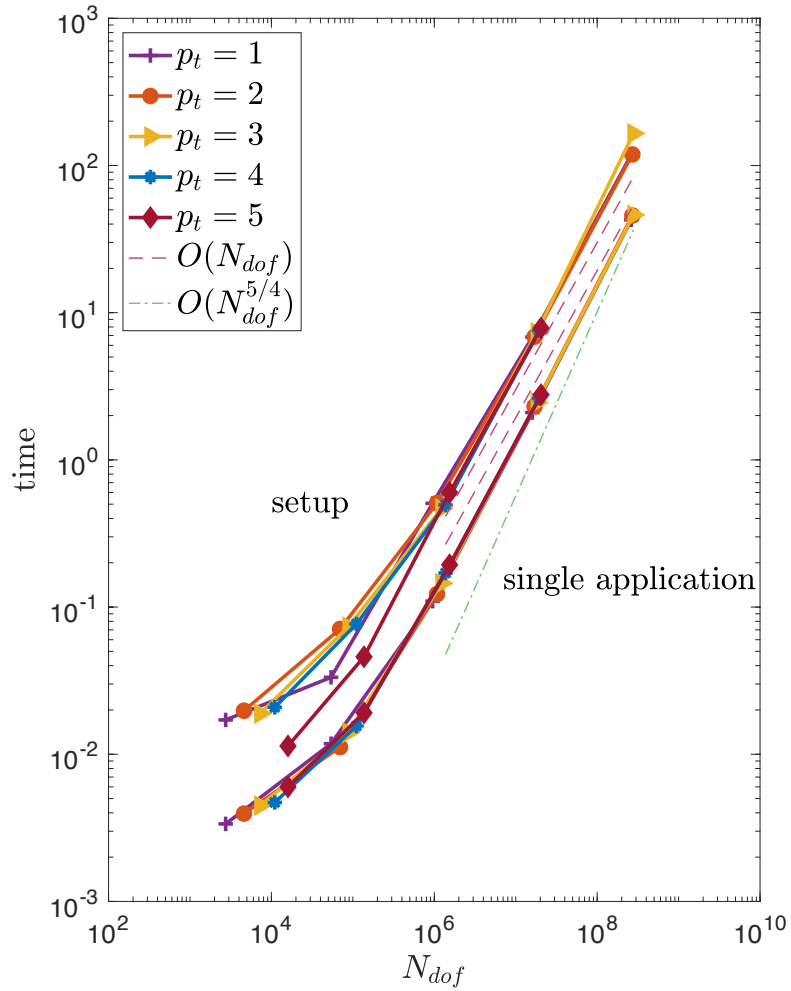


Figure 3: Setup time and single application time of  $\hat{\mathbf{A}}^G$  in the rotated quarter domain.

	$\hat{\mathbf{A}}$ Iterations / Time				
$n_{sub}$	$p = 1$	$p = 2$	$p = 3$	$p = 4$	$p = 5$
8	32 / 0.21	70 / 0.89	101 / 3.32	128 / 10.85	156 / 29.23
16	98 / 8.57	121 / 28.07	149 / 75.85	167 / 174.57	177 / 328.48
32	143 / 830.46	165 / 1653.22	177 / 2813.11	*	*

	$\hat{\mathbf{A}}^G$ Iterations / Time				
$n_{sub}$	$p = 1$	$p = 2$	$p = 3$	$p = 4$	$p = 5$
8	14 / 0.25	15 / 0.34	19 / 0.74	20 / 1.71	23 / 4.09
16	18 / 1.78	19 / 4.37	21 / 11.34	23 / 22.60	25 / 43.88
32	22 / 124.98	24 / 240.23	25 / 398.83	*	*

Table 7: Hollow torus domain. Performance of  $\hat{\mathbf{A}}$  and  $\hat{\mathbf{A}}^G$ .

exploits an ad-hoc factorization of the time matrices. The preconditioner cost seen in numerical tests, for a serial single core execution, is almost equal to  $O(N_{dof})$  and does not depend on the polynomial degree.

At the same time, the storage cost is roughly the same that we would have by discretizing separately in space and in time, if we assume  $n_t \leq Cp^d N_s$ . Indeed, in this case the memory used for the whole iterative solver is  $O(p^d N_s + N_{dof})$ .

The coupling with a matrix-free approach [25] will lead to a significant improvement of the solver strategy. Our method is also suited for parallelization and this will be an interesting future direction study.

## Acknowledgments

This research was partially supported by the European Research Council through the FP7 Ideas Consolidator Grant *HIGEOM* n.616563, and by the Italian Ministry of Education, University and Research (MIUR) through the “Dipartimenti di Eccellenza Program (2018-2022) - Dept. of Mathematics, University of Pavia”. The authors are members of the Gruppo Nazionale Calcolo Scientifico-Istituto Nazionale di Alta Matematica (GNCS-INDAM). This support is gratefully acknowledged.

## References

- [1] L. Beirão da Veiga, D. Cho, and G. Sangalli. Anisotropic NURBS approximation in isogeometric analysis. *Computer Methods in Applied Mechanics and Engineering*, 209:1–11, 2012.
- [2] J. Bonilla and S. Badia. Maximum-principle preserving space–time isogeometric analysis. *Computer Methods in Applied Mechanics and Engineering*, 354:422–440, 2019.
- [3] A. Bressan and E. Sande. Approximation in FEM, DG and IGA: a theoretical comparison. *Numerische Mathematik*, 2019, <https://doi.org/10.1007/s00211-019-01063-5>.
- [4] J. A. Cottrell, T. J. R. Hughes, and Y. Bazilevs. *Isogeometric analysis: toward integration of CAD and FEA*. John Wiley & Sons, 2009.
- [5] C. De Boor. *A practical guide to splines (revised edition)*. Applied Mathematical Sciences. Springer, Berlin, 2001.
- [6] M. O. Deville, P. F. Fischer, and E. H. Mund. *High-order methods for incompressible fluid flow*. Cambridge University Press, 2002.
- [7] C. A. Dorao and H. A. Jakobsen. A parallel time–space least-squares spectral element solver for incompressible flow problems. *Applied mathematics and computation*, 185(1):45–58, 2007.
- [8] J. A. Evans, Y. Bazilevs, I. Babuška, and T. J. R. Hughes.  $n$ -widths, sup-infs, and optimality ratios for the  $k$ -version of the isogeometric finite element method. *Computer Methods in Applied Mechanics and Engineering*, 198:1726–1741, 2009.
- [9] L. C. Evans. *Partial Differential equations*. American Mathematical Society, Berlin, 2010.
- [10] I. Fried. Finite-element analysis of time-dependent phenomena. *AIAA Journal*, 7(6):1170–1173, 1969.
- [11] K. P. S. Gahalaut, S. K. Tomar, and C. Douglas. Condition number estimates for matrices arising in NURBS based isogeometric discretizations of elliptic partial differential equations. *arXiv preprint arXiv:1406.6808*, 2014.
- [12] M. J. Gander. 50 years of time parallel time integration. In *Multiple Shooting and Time Domain Decomposition Methods*, pages 69–113. Springer, 2015.
- [13] M. J. Gander and M. Neumuüller. Analysis of a new space-time parallel multigrid algorithm for parabolic problems. *SIAM Journal on Scientific Computing*, 38(4):A2173–A2208, 2016.
- [14] C. Hofer, U. Langer, M. Neumuüller, and R. Schneckenleitner. Parallel and robust preconditioning for space-time isogeometric analysis of parabolic evolution problems. *SIAM Journal on Scientific Computing*, 41(3):A1793–A1821, 2019.

- [15] T. J. R. Hughes, J. A. Cottrell, and Y. Bazilevs. Isogeometric analysis: CAD, finite elements, NURBS, exact geometry and mesh refinement. *Computer Methods in Applied Mechanics and Engineering*, 194(39):4135–4195, 2005.
- [16] J. C. Bruch Jr and G. Zyyoloski. Transient two-dimensional heat conduction problems solved by the finite element method. *International Journal for Numerical Methods in Engineering*, 8(3):481–494, 1974.
- [17] T. G. Kolda and B. W. Bader. Tensor decompositions and applications. *SIAM review*, 51(3):455–500, 2009.
- [18] A. M. Kvarving and E. M. Rønquist. A fast tensor-product solver for incompressible fluid flow in partially deformed three-dimensional domains: Parallel implementation. *Computers & Fluids*, 52:22–32, 2011.
- [19] U. Langer, M. Neumüller, and I. Toulopoulos. Multipatch space-time isogeometric analysis of parabolic diffusion problems. In *International Conference on Large-Scale Scientific Computing*, pages 21–32. Springer, 2017.
- [20] R. E. Lynch, J. R. Rice, and D. H. Thomas. Direct solution of partial difference equations by tensor product methods. *Numerische Mathematik*, 6(1):185–199, 1964.
- [21] M. Montardini, M. Negri, G. Sangalli, and M. Tani. Space-time least-squares isogeometric method and efficient solver for parabolic problems. *Mathematics of Computation (accepted for publication)*, 2019.
- [22] M. Montardini, G. Sangalli, and M. Tani. Robust isogeometric preconditioners for the Stokes system based on the Fast Diagonalization method. *Computer Methods in Applied Mechanics and Engineering*, 338:162 – 185, 2018.
- [23] J. T. Oden. A general theory of finite elements. II. Applications. *International Journal for Numerical Methods in Engineering*, 1(3):247–259, 1969.
- [24] G. Sangalli and M. Tani. Isogeometric preconditioners based on fast solvers for the Sylvester equation. *SIAM Journal on Scientific Computing*, 38(6):A3644–A3671, 2016.
- [25] G. Sangalli and M. Tani. Matrix-free weighted quadrature for a computationally efficient isogeometric k-method. *Computer Methods in Applied Mechanics and Engineering*, 338:117 – 133, 2018.
- [26] F. Shakib and T. J. R. Hughes. A new finite element formulation for computational fluid dynamics: IX. Fourier analysis of space-time Galerkin/least-squares algorithms. *Computer Methods in Applied Mechanics and Engineering*, 87(1):35–58, 1991.
- [27] L. Sorber, M. Van Barel, and L. De Lathauwer. Tensorlab v2. 0. Available online, URL: [www.tensorlab.net](http://www.tensorlab.net), 2014.
- [28] O. Steinbach. Space-time finite element methods for parabolic problems. *Computational methods in applied mathematics*, 15(4):551–566, 2015.
- [29] R. Stevenson and J. Westerdiep. Stability of Galerkin discretizations of a mixed space-time variational formulation of parabolic evolution equations. *arXiv:1902.06279*, 2019.
- [30] K. Takizawa, T. E. Tezduyar, Y. Otoguro, T. Terahara, T. Kuraishi, and H. Hattori. Turbocharger flow computations with the space-time isogeometric analysis (ST-IGA). *Computers & Fluids*, 142:15–20, 2017.
- [31] K. Takizawa, T. E. Tezduyar, and T. Terahara. Ram-air parachute structural and fluid mechanics computations with the space-time isogeometric analysis (ST-IGA). *Computers & Fluids*, 141:191–200, 2016.
- [32] K. Takizawa, T. E. Tezduyar, T. Terahara, and T. Sasaki. Heart valve flow computation with the space-time slip interface topology change (ST-SI-TC) method and isogeometric analysis (IGA). In *Biomedical Technology*, pages 77–99. Springer, 2018.
- [33] R. Vázquez. A new design for the implementation of isogeometric analysis in Octave and Matlab: GeoPDEs 3.0. *Computers & Mathematics with Applications*, 72(3):523–554, 2016.